GEOCHRONOMETRIA 52 (2025) 205688
DOI 10.20858/geochr/205688

Available online at https://www.geochronometria.com/

A FIRST CHRONOLOGICAL FRAMEWORK FOR FLUVIAL TERRACE DEPOSITS OF THE KAMPAR KANAN RIVER, INDONESIA

YUNIARTI YUSKAR[1, 4], MELANIE KRANZ-BARTZ[3], CHRISTOPH SCHMIDT[1], TIGGI CHOANJI[2, 4], STUART N. LANE[1] and GEORGINA E. KING[1]

[1]*Institute of Earth Surface Dynamics, University of Lausanne, 1015 Lausanne, Switzerland*
[2]*Institute of Earth Science, University of Lausanne, 1015 Lausanne, Switzerland*
[3]*Institute of Geosciences, Ruhr University Bochum, 44801 Bochum, Germany*
[4]*Department of Geological Engineering, Universitas Islam Riau, 28284 Pekanbaru, Indonesia*

Received 31 December 2024 Accepted 28 May 2025

Abstract
Late Quaternary landscape evolution in tropical environments, such as Indonesia, remains poorly constrained due to limited prior studies and mineral properties that are challenging for luminescence dating. In this study, single- and multi-grain luminescence measurements of quartz and K-feldspar were explored for fill terrace deposits at the Kampar Kanan River, Indonesia. Our objective is to develop a chrono-stratigraphic framework that allows the reconstruction of late Quaternary fluvial morpho-dynamics, including climatic change. Quartz measurements were made using blue and green stimulation and single-aliquot regenerative dose (SAR) and double SAR protocols. However, as none of the quartz signals were fast component-dominated, they were not used for dating. Infrared-stimulated luminescence of multiple grains of K-feldspar at 50°C (IR_{50}) and post-infrared infrared-stimulated luminescence at 225°C ($pIR_{50}IRSL_{225}$) yielded sufficiently bright signal intensities for dating, and ages were calculated using either the average dose (ADM) or minimum age model (MAM). The luminescence chronology based on fading corrected $pIR_{50}IRSL_{225}$ data yields ages from Marine Isotope Stage (MIS) 6 or earlier to MIS 1. The chrono-stratigraphy indicates that the river was likely aggradational during climate transitions from wet to dry with the deposition of more gravelly material, and erosional during colder periods when overbank deposition of fines may have been coincident with increased vertical river erosion due to a stronger monsoon.

Keywords
Luminescence dating, K-Feldspar IRSL, Quaternary, fluvial, Indonesia

1. Introduction

Fluvial archives are key for studying paleo-environmental changes linked to Quaternary climatic fluctuations (e.g., Macklin *et al.*, 2012; Bridgland and Westaway, 2008). During the Quaternary, large-scale climate forcing resulted in glacials and interglacials, which are characterized by cold and warm climates in the high- and mid-latitutes, and generally drier and wetter conditions in the low latitutes (Macklin *et al.*, 2012). Tropical climates are commonly associated with equatorial convective rainfall and monsoon-influenced precipitation, giving rise to mostly wet conditions punctuated by short dry seasons (Syvitski *et al.*, 2014). The tropical rivers of Southeast Asia and India are renowned for widespread and frequent flooding, which is related to significant discharge during wet seasons (Heitmuller and Hudson, 2009; Mishra and Sinha, 2020). Seasonal precipitation changes, reflected in annual rainfall totals are known to have changed fluvial activity during glacial periods in tropical lowland areas such as Indonesia (Verstappen, 1980; Thorp and Thomas, 1992; Thomas, 2008). However, the relationships between such climatic changes and direct (discharge-related) as well as indirect (sediment supply and runoff) impacts on fluvial morphodynamics remain poorly constrained, especially in

Corresponding author: Y. Yuskar
e-mail: yuniarti.yuskar@unil.ch

ISSN 1897-1695 (online), 1733-8387 (print)

tropical environments during the Pleistocene–Holocene transition (Thomas, 2008).

Tropical rivers, particularly those draining tectonically active mountain belts, transport significant quantities of material that may be deposited on floodplains, and those deposits are excellent geo-archives for reconstructing environmental change (Sinha and Latrubesse, 2020). However, the fluvial dynamics of tropical rivers are challenging to constrain due to their complex depositional histories that reflect non-stationary environmental forcing and associated autogenic responses (Sinha *et al.*, 2012). Understanding the timing and dynamics of episodic changes in tropical floodplains has been a long-term challenge in fluvial geomorphology (Knox, 2006), not least because of interactions between discharge, slope, climate, and vegetation (e.g., Stanistreet *et al.*, 1993) in controlling the river channel forms, patterns and depositional/erosion histories.

The focus of this paper is the Kampar Kanan river catchment in Sumatra Island, Indonesia. This Kampar river is not only one of Indonesia's most important ones, it is also located in a climate zone highly sensitive to climate events and changes (e.g., El Niño Southern Oscillation (ENSO), Monsoon) (Kausarian *et al.*, 2024). The aim of the wider project is to understand the direct and indirect effects of late Quaternary climate change upon the fluvial dynamics of the Kampar river. To do this, a robust chronology is essential to set Quaternary fluvial dynamics in relation to environmental change (e.g., Riebe *et al.*, 2000; Cunha *et al.*, 2008). However, establishing reliable chronostratigraphies of fluvial deposits is generally challenging given the heterogeneous nature of river deposits and long time-scales required for fluvial response such as for example terrace formations (Rixhon *et al.*, 2017). The timing of major fluvial responses in Indonesia is remarkably understudied. Only a few studies exist that report quantitative ages due to the difficulties of dating ancient Quaternary deposits in tropical environments. Across the Indonesian archipelago, (Kaharudin *et al.*, 2020) reported radiocarbon ages related to archaeological sites, including caves and rock shelters. However, radiocarbon dating in humid regions can be complicated due to oxidation of organic matter and reworking of old carbon in fluvial sediments (Blong and Gillespie, 1978; Stanley, 2000; Wood *et al.*, 2008). Consequently, Late Pleistocene radiocarbon dates in Indonesia are usually determined from shells (Louys *et al.*, 2017; Morley, 2017). Alternative dating techniques such as optical stimulated luminescence (OSL) dating of sediment which and U-series dating of bone-bearing and speleothems, combined with electron spin resonance (ESR) dating on human and faunal teeth, have been applied to archaeological sites in West Sumatra, Indonesia (Westaway *et al.*, 2017; Kaharudin *et al.*, 2020), although such studies are limited in number.

Luminescence dating represents a potentially excellent dating tool for constraining the timing of fluvial sediment deposition (Rittenour, 2008). However, Indonesia is known to be a challenging location for the application of luminescence dating (Westaway and Roberts, 2006) and previous studies for sites at Timor, Flores, Java and Sulawesi have found that the blue-stimulated UV-emission of quartz lacks a fast component and has an unstable medium component that can result in age underestimation (Westaway, 2009). Nonetheless, single-grain and single-aliquot quartz (Westaway, 2009) and K-feldspar analyses (Westaway, 2009; Sutikna *et al.*, 2016; Van Den Bergh *et al.*, 2016; Sontag-González *et al.*, 2021; O'Gorman *et al.*, 2021) from the same locations have yielded dates commensurate with independent age controls. More recent work in the Padang highlands, West Sumatra, presented promising K-feldspar luminescence dates (Westaway *et al.*, 2017; Duval *et al.*, 2021).

Against this background, this study aims (i) to develop a chronology of the Kampar river deposits using different luminescence dating techniques; and (ii) to determine over the late the timing of aggradation and incision phases in response to changing climate. Given the difficulties of using luminescence dating in Indonesia and in tropical environments in general, we study in detail OSL and post-infrared stimulated luminescence (pIR-IRSL) signals of quartz and K-feldspar minerals, respectively, with the goal to establish a luminescence measurement protocol for dating tropical (river) deposits.

2. Study Area

The Kampar Kanan River with a catchment size of 24,550 km^2 is located in the centre of Sumatra Island, Indonesia and flows from its headwaters in the Barisan mountains of West Sumatra to its outlet on the island's eastern coast, into Malacca Strait (**Fig. 1a**). It has a length of ~580 km and is one of the largest rivers in Sumatra with an appoximate mean annual discharge of 600 m^3 s^{-1} (Wisha *et al.*, 2018; Wisha *et al.*, 2022), and is prone to periodic flooding due to its typical meandering morphology (**Fig. 1b**). The study area is located in the Indo-Pacific Warm Pool (IPWP) oceanic zone and is influenced by the East Asian monsoon and the ENSO (Linsley *et al.*, 2010). Based on rainfall data from 2018 to 2023, the Kampar Kanan River catchment experiences average precipitation of between 130 and 560 mm month^{-1} (Kausarian *et al.*, 2024).

This river is also part of the Central Sumatra Basin (CSB) that during the Middle Miocene up to recent times underwent a compressional phase, involving WSW-directed thrusting and reverse faulting along reactivated NNW-striking wrench faults, SSW-verging monoclinal flexuring above NW-WNW basement breaks, and transtensional rifting along N-NNE-trending elements (Hendrick and Aulia, 1993; Yuskar *et al.*, 2017). The upper catchment area of the Kampar Kanan River is characterized by Tertiary rocks that have undergone tectonic uplift (Koesoemadinata and Matasak, 1981; Putra and Choanji, 2016; Choanji, 2019) and the sediments forming the terraces of the Kampar Kanan River are sourced from the

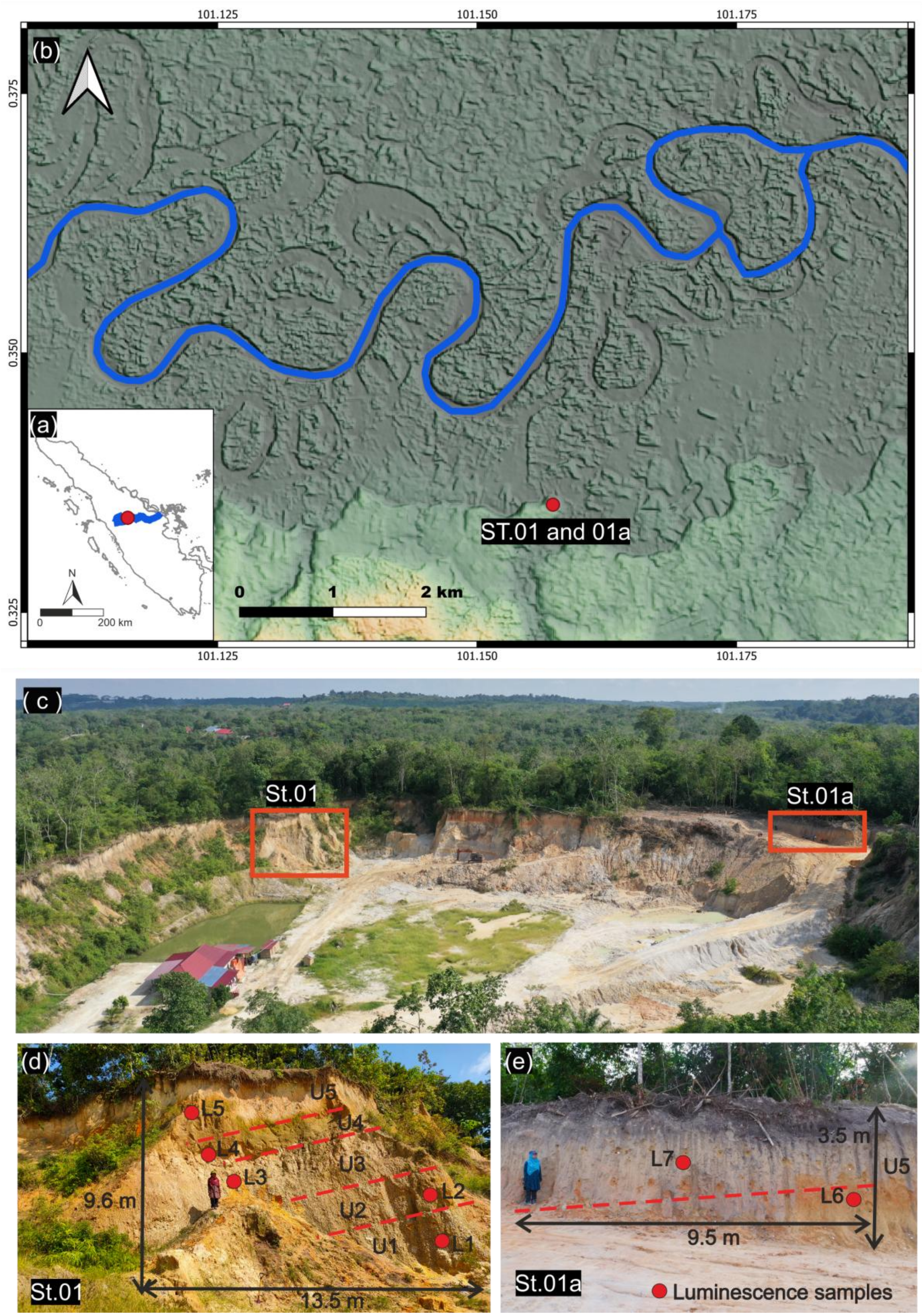

Fig. 1. *Research area at the Kampar Kanan River, Riau Province in Sumatra Island – Indonesia. Sample locations are indicated with their names.* ***(a)*** *Sumatra Island – Indonesia, the red dot shows the research location.* ***(b)*** *Kampar Kanan River and surroundings (modified from DEMNAS 8 m resolution), the red dot shows St.01 and 01a.* ***(c)*** *The terraces and site location of St. 01 and 01a.* ***(d)*** *and* ***(e)*** *show a zoom-in on site 01 and 01a, red dots show the luminescence sampling locations.*

Bahorok Formation (Pub; metasediment rocks), Pematang Formation (Tlpe; red and mottled mudstones, breccio-conglomeratic, conglomeratic sandstones), Sihapas Formation (Tms; conglomeratic sandstones and siltstones), and Telisa Formation (Tmt; siltstones, sandstones, mudstones), and Petani Formation (Tup; mudstones, siltstones and sandstones) (Clarke *et al.*, 1982; Choanji, 2019, 2017). Based on the regional geological map of the sheet Pekanbaru, the sedimentary deposits of the Kampar Kanan River are categorised as the Minas Formation (Qpmi), Older Alluvium (Qp) and Younger Alluvium (Qh) (Clarke *et al.*, 1982). Gravels, pebble spreads, sands and clays make up the Qpmi Formation (Clarke *et al.*, 1982). The Qp is characterized by gravels, sands, clays, and organic materials (Clarke *et al.*, 1982; Yuskar, 2016), likely deposited in the Pleistocene to Holocene (Clarke *et al.*, 1982), whereas the Qh deposits consist of gravels, sands and clays that were deposited during the Holocene (Clarke *et al.*, 1982; Yuskar, 2016; Yuskar *et al.*, 2018; Revanda *et al.*, 2019).

Our study area is located in the upper reaches of the Kampar Kanan River (**Fig. 1**). One representative fluvial sedimentary sequence, located approximately 32 km from the source and approximately 1.2 km south of modern channel (**Fig. 1a–1e**), was chosen to explore the luminescence properties of river deposits and to develop a luminescence measurement protocol for dating tropical river purposes. A ~13 m-thick composite sediment section (i.e., from two correlable fluvial sections based on their sedimentology, namely St. 01 and St. 01a; **Fig. 2**) were investigated that can be subdivided into five main units (from bottom to top), see **Fig. 1c-1e**. Unit 1 (U1) is characterized by massive sediment with yellowish grey-weathered and grey-fresh colours, massive rounded to sub-rounded cobbles and gravels, supported in a matrix of medium to coarse sand with silica cement. Unit 2 (U2) shows brownish-yellow weathered colour and yellow fresh colour and consists of sub-rounded to rounded pebbles and coarse sand matrix cemented with silica. The fining-upward sediment of unit 3 (U3) contained sediment with reddish grey-weathered and yellowish brown-fresh colours, sub-rounded to rounded granule and pebble grains, grains supported into medium – fine sand and a silica cement. Unit 4 (U4) is identified by fining-upward reddish grey-weathered and blackish yellow-fresh colours with pebbles in fine to medium sand, matrix-supported and silica-cemented. Unit 5 (U5) is covered by soil. This unit is designated by yellowish-red weathered and yellowish-brown fresh colours of fine to medium sand with roots, being matrix supported with silica cement.

3. Methodology

3.1. Sampling, sample preparation and characterization

In total, seven luminescence samples were collected from the different stratigraphic units (U1-U5): Samples L1 (8.4 m b.s.), L2 (7.0 m b.s.), L3 (5.5 m b.s.), L4 (3.0 m b.s.), and L5 (1.5 m b.s.) were collected from U1, U2, U3, U4, and U5, respectively, from site St.01 (49 m a.s.l.), whilst samples L6 (1.6 m b.s.) and L7 (2.4 m b.s.) were additionally taken from U5 from site St.01a (55 m a.s.l.) (**Table 1**). Luminescence samples were collected by hammering cylindrical steel tubes (25 cm long, 6 cm in diameter) into the freshly cleaned sections. The surrounding sediment was collected for measurement of the dose rate which was done using high-resolution gamma-spectrometry (HRGS) at the luminescence laboratory at the University of Lausanne (UNIL, Switzerland).

All luminescence samples were opened under subdued red-light conditions at UNIL. After drying at 40°C, samples were sieved to obtain the coarse-grained fraction (90–250 µm) and then treated with hydrochloric acid (HCl, 10%) to remove carbonates and hydrogen peroxide (H_2O_2, 35%) to remove organic matter. Density separation using sodium polytungstate was conducted to extract the quartz-rich (2.62–2.70 g cm^{-3}) and K-feldspar-rich fraction (<2.58 g cm^{-3}). The resulting quartz and K-feldspar fractions were sieved to 180–212 µm, whilst we used the 100–250 µm grain size fraction for the K-feldspar extract of samples L6 and L7 due to an insufficient number of K-feldspar grains in 180–212 µm grain size range. The quartz fraction was etched with hydrofluoric acid (HF, 40%) for 40 min plus a final HCl (10%) wash. No HF treatment was used for the K-feldspar fraction (Duller, 1992).

We carried out additional analyses to check the purity of our quartz and K-feldspar samples. Scanning Electron

Table 1. *Summary of dose rate measurements. Secular equilibrium in the ^{238}U decay chain has been observed.*

Sample code	Radioelement concentrations			Depth of sampling (m)	Thickness of layer (m)	Water content (wt.%)	Environmental dose rate (Gy ka^{-1})
	U (µg g^{-1})	Th (µg g^{-1})	K (%)				
L7	1.7 ± 0.1	7.8 ± 0.5	0.18 ± 0.03	1.6	1.6	13.6	1.71 ± 0.19
L6	1.8 ± 0.2	7.9 ± 0.5	0.11 ± 0.02	2.4	2.4	11.3	1.74 ± 0.19
L5	2.2 ± 0.3	11.2 ± 1.2	0.18 ± 0.02	1.5	1.5	13.8	1.88 ± 0.08
L4	1.2 ± 0.1	5.5 ± 0.2	0.07 ± 0.01	3.0	3.5	9.3	1.42 ± 0.06
L3	1.5 ± 0.1	7.5 ± 0.5	0.14 ± 0.02	5.5	6.7	15.5	1.41 ± 0.06
L2	2.2 ± 0.2	11.9 ± 0.5	0.79 ± 0.07	7.0	8.6	21.2	2.17 ± 0.08
L1	0.7 ± 0.1	3.5 ± 0.2	0.26 ± 0.03	8.4	10.4	6.7	1.22 ± 0.05

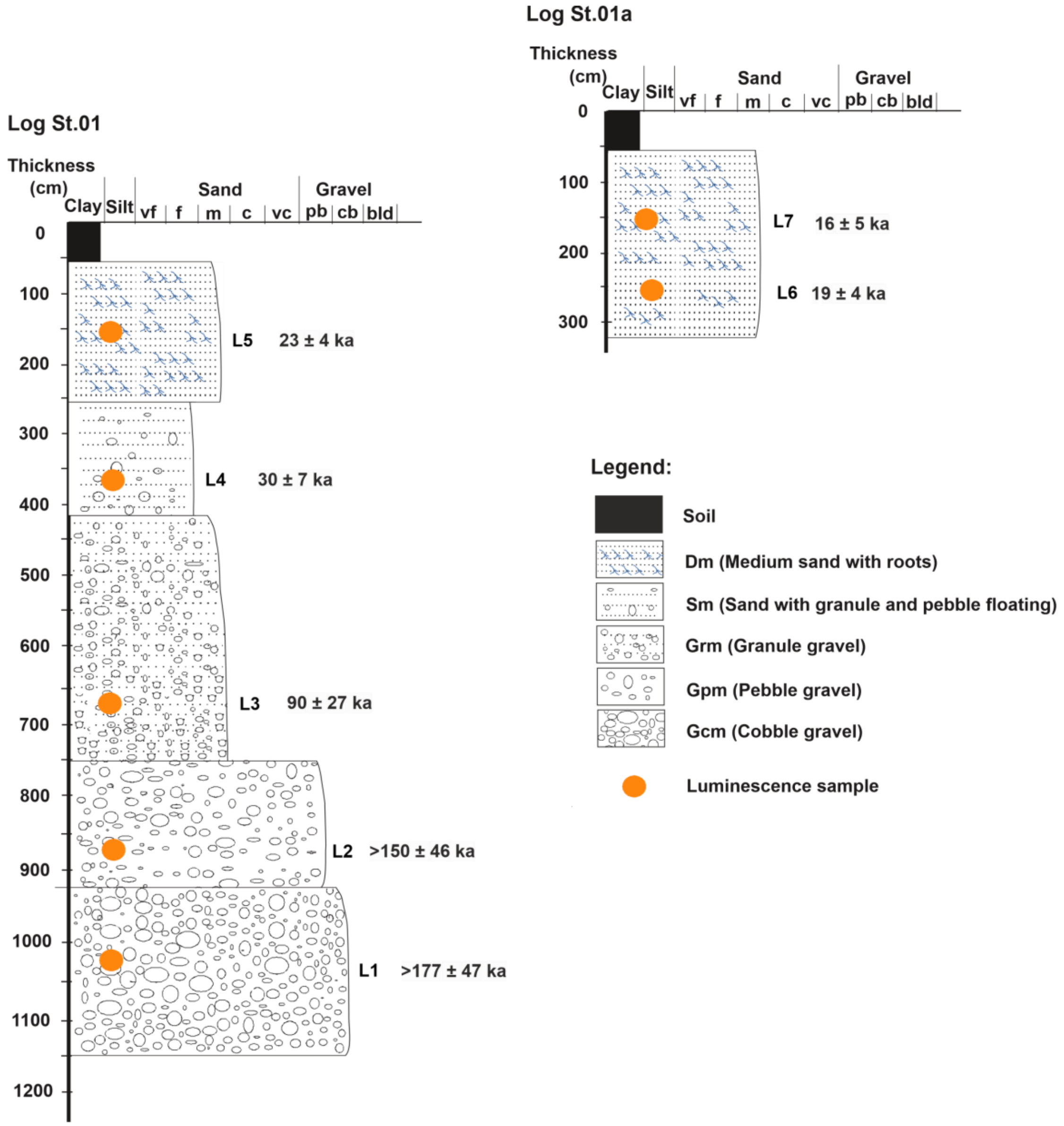

Fig. 2. *Log of St.01 and St.01a, including all units and sediment facies (classification by Krüger and Kjær, 1999 as modified from Miall, 1985). Sample numbers and the resultant luminescence ages (fading-corrected $pIR_{50}IRSL_{225}$ MAM ages are displayed for L1 to L7 with the exception of L6 for which the fading-corrected $pIR_{50}IRSL_{225}$ ADM age is given; see **Table 2**).*

Microscopy (SEM) analyses were done to check for the contamination of quartz grains with other minerals. The number of K-feldspar grains in the <2.58 g cm^{-3} density fraction was quantified using a binocular microscope and Raman spectroscopy. Raman spectroscopy is used to identity minerals and their polymorphic forms (see **Table S1** for instrument details and results). In addition, an X-Ray Fluorescence (XRF) attachment to the Risø TL/OSL reader allowed us to identify the specific mineralogy of multi-grain (MG) K-feldspar aliquots (Qz = SiO_2, Ab = $NaAlSi_3O_8$, An = $CaAl_2Si_2O_8$, Or = $KAlSi_3O_8$) with an estimated analytical precision of 7% (Guralnik *et al.*, 2015); see **Fig. S1** and **Table S2** for full XRF results.

3.2. Luminescence measurements and D_e determination

Luminescence measurements were performed using two automated Risø TL/OSL-DA-20 readers equipped with $^{90}Sr/^{90}Y$ beta sources with dose rates of ~0.10 Gy s^{-1} and ~0.19 Gy s^{-1}, respectively (calibrated with Risø calibration quartz batch 200; Hansen *et al.*, 2015; Autzen *et al.*, 2022). MG analyses were carried out using small aliquots (2 and 3 mm in diameter). The 180–212 µm (L1 to L5 samples) and 100–250 µm (L6 and L7 samples) grain size fractions were loaded into 300 µm diameter hole single-grain discs for single-grain (SG) measurements. Visual control showed that occurrences of multiple grains in one hole were infrequent (<1%).

Quartz luminescence measurements were made following a single-aliquot regenerative (SAR) dose protocol (Murray and Wintle, 2000). Quartz luminescence emissions were detected through a 7.5 mm Hoya U340 filter. Previous studies have highlighed the difficulties of isolating the fast component and feldspar contamination of quartz samples from Indonesia (Westaway, 2009). Consequently, we tested different measurement approaches including blue (Murray and Wintle, 2000) and green light stimulation (Bailey *et al.*, 2015), and a double SAR protocol where infrared (IR) stimulation preceeds the blue or green stimulation (Banerjee *et al.*, 2001; Roberts and Wintle, 2001; Zhang and Zhou, 2007). An IR depletion test with an acceptance threshold of 10% was included in the final SAR cycle to screen for feldspar contamination (Duller, 2003); see **Table S3** for details of the measurement protocols. Representatitive signals of different aliquots measured using blue and green stimulation were used for continuous wave (CW)- and linearly modulated (LM)-OSL deconvolution analyses to check for the fast component contribution (see further details in the supplement).

Feldspar minerals were measured using a pIR-IRSL (Thomsen *et al.*, 2008; Buylaert *et al.*, 2009) protocol with a first stimulation at 50°C (180 s) and a second stimulation at 225°C (180 s) after a preheat of 250°C (60 s). At the end of each $pIR_{50}IRSL_{225}$ measurement cycle, a high-temperature IR wash at 290°C for 100 s was used (**Table S3**). IRSL emissions were detected using a blue filter pack (3 mm Schott BG3 and 3 mm Schott BG39 filters). The IR power delivered to the sample position was 90% of the maximum power (~140 mW cm^{-2}). Regenerative doses between 46 and 684 Gy were used for dose-response curve construction, and the test dose was 57 Gy. Six further aliquots of samples L1, L4, L5 and L6 were bleached using a solar simulator (Hönle UVACube400) for 24 h. From these samples, three aliquots were used for a dose recovery test following a laboratory dose of 84 Gy, the three remaining aliquots were measured to determine the residual dose. We applied signal integration limits of the first 8 s and background integration of the final 27 s for all signals.

Anomalous fading experiments were carried out on three previously measured aliquots for each sample. Samples were irradiated with a given dose of 110 Gy and preheated prior to storage (Auclair *et al.*, 2003), the test dose was 55 Gy and delay times were 1.7, 3.3, 6.7, and 13.3 h. The initial delay time measurement was repeated. We calculated fading rates using the `analyse_FadingMeasurement()` function 0.1.21 in the R package 'Luminescence' (v0.9.22; Kreutzer *et al.*, 2012; Kreutzer and Burow, 2023). Fading rates were normalised to a delay time of 2 days (g_{2days}; Huntley and Lamothe, 2001) and the average fading rate of the three aliquots was used for fading correction using the approach of Huntley (2006) and Kars *et al.* (2008).

For quartz and feldspar measurements, the following acceptance criteria were adopted: recycling ratio within 10% of unity and recuperation below 5% (Murray and Wintle, 2000); signal >3σ above background; and $D_e < 2D_0$. In the case of K-feldspar samples, $D_e < 2D_0$ is not an effective screening criterion where no anomalous fading correction has been made (King *et al.*, 2018). Therefore, we tested whether our feldspar samples were in field saturation by comparing the natural level of trap filling (n/N) with that predicted for athermal steady-state ($(n/N)_{ss}$) using the `calc_Huntley2006()` function 0.4.1 in the R package 'Luminescence' (v0.9.22 ; King and Burow, 2023). We used a single-saturating exponential fit (1EXP, after Kars *et al.*, 2008). Depending on the shape of the D_e distribution, we applied either the minimum age model (MAM) of Galbraith *et al.* (1999) or the average dose model (ADM; Guérin *et al.*, 2017) to calculate ages for samples considered to have been well bleached or partially bleached prior to burial (Smedley *et al.*, 2019). In the MAM, sigma-b (σ_b) is the excess D_e value dispersion that would be anticipated if a sample had been well-bleached (Cunningham and Wallinga, 2012). The σ_b of samples from well-bleached settings has been found to cover a range of values from 0.2 to 0.4 (Smedley *et al.*, 2019). As a modern analogue is not available for the samples from sites St.01 and St.01a, we selected a σ_b value of 0.3 for the MAM. Age modelling using the MAM or ADM was undertaken using the using the `calc_MinDose()` functions 0.4.4 (Burrow, 2023) and `calc_AverageDose()` functions 0.1.5 (Christophe *et al.*, 2023) in the R package 'Luminescence' (v0.9.22; Kreutzer *et al.*, 2023).

3.3. Dose rate determination

Dose rate samples were milled and sealed in beakers for at least four weeks prior to measurement using HRGS. The environmental dose rate of the sample was calculated using DRAC (v1.2; Durcan *et al.*, 2015) using the conversion factors of Guérin *et al.* (2011), and the beta grain size attenuation factors of Guérin *et al.* (2012). An alpha efficiency value of 0.15 ± 0.05 was assumed for feldspar (Balescu and Lamothe, 1994). The cosmic dose rate was assessed following Prescott and Hutton (1994). We used an average internal K content based of 8.43% on XRF measurements from all samples (**Table S2**). The water content was calculated as the percentage of the weight of water (wet mass – dry mass) divided by the dry sediment mass for all samples (Durcan *et al.*, 2015).

4. Results

4.1. Quartz OSL signal properties

Scanning Electron Microscopy – Energy Dispersive X-ray Spectroscopy (SEM-EDS) analyses of the samples show no feldspar contamination in the quartz extracts (based on morphology, colour and composition). However, blue stimulated quartz luminescence signals were not fast component-dominated (**Fig. S2** and **Fig. S3**). Green LED stimulation yielded similar results and a measurable fast component could not be isolated for dating the Kampar Kanan River samples. Furthermore, multiple aliquots failed the IR depletion test. Double SAR measurements and a second HF treatment were done to try to remove the IR-sensitive signal; however, this was also unsuccessful (continued IR sensitivity), and no fast component could be isolated from the post-IR blue stimulated signal. Examples of signal decay curves using different measurement protocols are shown in **Fig. 3**. SG quartz analyses yielded an acceptance rate of <1% which meant that they were impractical. As it was not possible to isolate a fast component or non-IR responsive signal from the quartz extracts, measurements on this mineral fraction were discontinued.

4.2. K-feldspar pIR$_{50}$IRSL$_{225}$

4.2.1. Signal properties and D_e determination

Raman spectroscopy of MG K-feldspar extracts of samples L1, L3 and L6 indicate that only 1% (200 grains analysed, L1) to 5% (75 grains analysed, L3 and L6) of grains are K-feldspar (see **Table S1**). This implies that for MG aliquots of K-feldspar, only a few grains contribute to the luminescence signal. The total number of grains on a 3 mm diameter aliquot was estimated for the 180–212 µm (samples L1 to L5) and 100–250 µm (samples L6 to L7) grain size ranges based on manual counting and the function `calc_AliquotSize()` functions 0.31 in the R package 'Luminescence' (v1.01; Burow, 2025). Each aliquot consists of 135–200 and 200–300 grains, showing that only 1–5 grains on a MG aliquot contribute to the measured luminescence signal, and probably only a single grain for sample L1. Overall, K-feldspar MG analyses yielded sufficient IRSL signal intensities for D_e measurement (i.e., 10^2–10^3 cts/0.77 s; **Fig. 4** and **Fig. S4**).

The XRF data are consistent with the Raman results and show that only 1–5% of the grains in a MG K-feldspar aliquot are feldspar (see **Table S2**). Assuming a 12.5% K content for K-feldspar (Huntley and Baril, 1997), we estimated the effective K content of the measured feldspar grains based on the relative proportions of Na-feldspar and K-feldspar, as obtained from the XRF analyses (see **Table S2** and **Fig. S1**). The results show that the average K content for the K-feldspar extract of all samples is ~8%, a value we applied to estimate the environmental dose rate. In total, 48 aliquots of all samples (L1 to L7 samples) were measured for D_e evaluation, with the exception of sample L2 for which we measured 32 aliquots due to a lack of material. The aliquot acceptance rate ranged from 40 to 95% for the IR$_{50}$ signal and from 20 to 90% for pIR$_{50}$IRSL$_{225}$ signals. The main reason for aliquot rejection was poor recycling and high recuperation. Dose-response curves were best fitted using a single saturating exponential function (**Fig. 4** and **Fig. S4**).

Mean residual doses from three aliquots each of samples L1, L4, L5 and L6 span the range of ~0.7–1.9 Gy (IR$_{50}$) and ~0.8–4.4 Gy (pIR$_{50}$IRSL$_{225}$) and represent <1% of the natural single-aliquot pIR$_{50}$IRSL$_{225}$ D_e values. Residual subtracted dose recovery ratios were within 10–15% of unity for the IR$_{50}$ and pIR$_{50}$IRSL$_{225}$ signals, indicating that the selected measurement protocol is appropriate (see **Fig. 5**).

D_e distributions of samples L1 to L7 yielded significant scatter and an asymmetric distribution of D_e values (**Fig. 6** and **Fig S5**) with overdispersion (OD) values between 21 and 92% (**Table 2**). The IR$_{50}$ and the pIR$_{50}$IRSL$_{225}$ signals

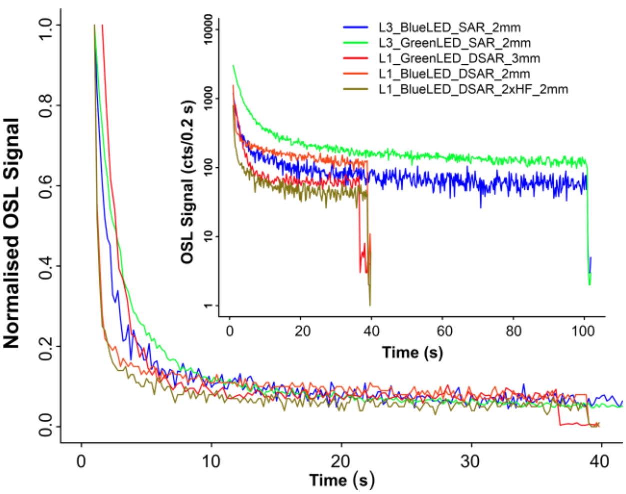

Fig. 3. *Quartz OSL signal decay curves for samples L1 and L3 following stimulation with blue, green or post-IR blue light in the course of SAR and double SAR protocols. Aliquot sizes are indicated, and one measurement is followed by two HF treatments (2 x HF). The main plot presents the OSL signal normalized to unity, and the inset plot displays the measured OSL signal.*

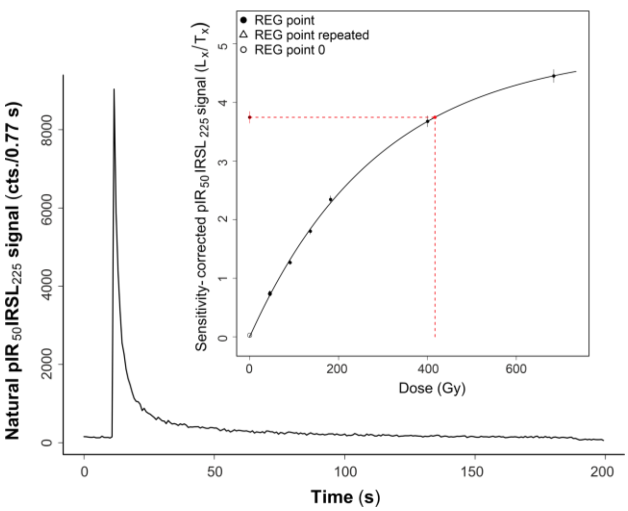

Fig. 4. *MG K-feldspar pIR$_{50}$IRSL$_{225}$ decay curve and dose-response curve (DRC) of sample L3. The red circle denotes the sensitivity-corrected natural pIR$_{50}$IRSL$_{225}$ signal (L_n/T_n), whilst the black circles show the regenerative (REG) dose points (L_x/T_x).*

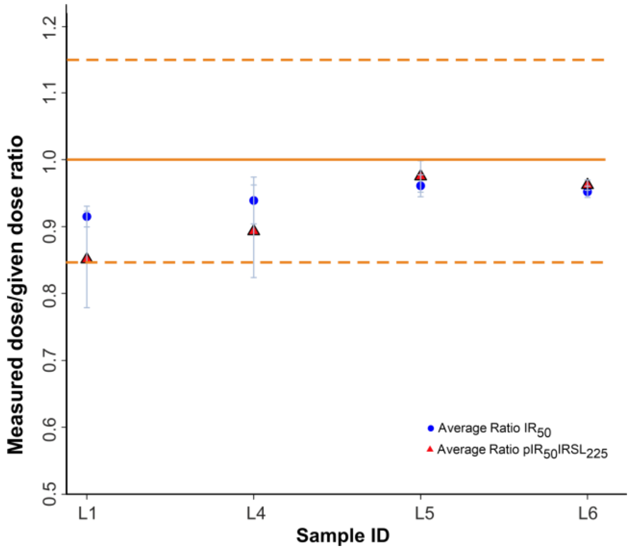

Fig. 5. *Residual-subtracted dose recovery ratio results for MG K-feldspar of samples L1, L4, L5 and L6. The solid line indicates unity, whilst the dashed lines indicate 15% deviation from unity.*

show similar dose distribution patterns. Most of the samples are characterized by positive skewness (**Fig. 6**) with the exception of the IR_{50} signal of L3 and the $pIR_{50}IRSL_{225}$ signals of L2 and L4 that show weak negative skewness (**Fig. 6** and **Fig. S5**).

We explored the effect of OD on sample ages by computing MAM D_e values using σ_b values of between 0.2 and 0.4 (Smedley *et al.*, 2019). D_e results were broadly consistent irrespective of the σ_b value used, but increase with increasing σ_b, see **Table S4**. Sample L6 ($pIR_{50}IRSL_{225}$) has an OD of 21%, indicative of complete bleaching (e.g. Choi *et al.*, 2024) and thus, the ADM was used to determine the $pIR_{50}IRSL_{225}$ age of this sample. Ages of all samples were also computed using the ADM for comparative purposes.

For the IR_{50} signal, fading-uncorrected D_e values range between 8.9 ± 0.8 Gy and 361.4 ± 28.2 Gy (ADM) compared to 4.8 ± 0.9 Gy and 345.0 ± 48.5 Gy (MAM), and for the $pIR_{50}IRSL_{225}$ signal, fading-uncorrected D_e values range between 27.8 ± 0.9 Gy and 478.1 ± 65.7 Gy (ADM) compared to 18.0 ± 2.6 Gy and 307.7 ± 87.8 Gy (MAM), see **Table 2**. The ADM yielded systematically higher D_e values compared to those calculated using the MAM.

4.2.2. Fading rates

Measurement of the *g*-values for these samples was challenging due to their poor luminescence brightness and high heterogeneity in *g*-values between aliquots. We tested different maximum delay times (13.33 and 26.67 h), which did not change the results. The results of the fading tests are summarized in **Table 2** and **Fig. S6**. Mean g_{2days}-values ranged from 0.87 ± 0.71 to 7.87 ± 3.22 %/decade for the IR_{50} signal whereas fading rates for the $pIR_{50}IRSL_{225}$ were lower with g_{2days}-values varying between 0.35 ± 0.70 and 3.99 ± 1.49 %/decade. Comparing the natural signals (n/N)

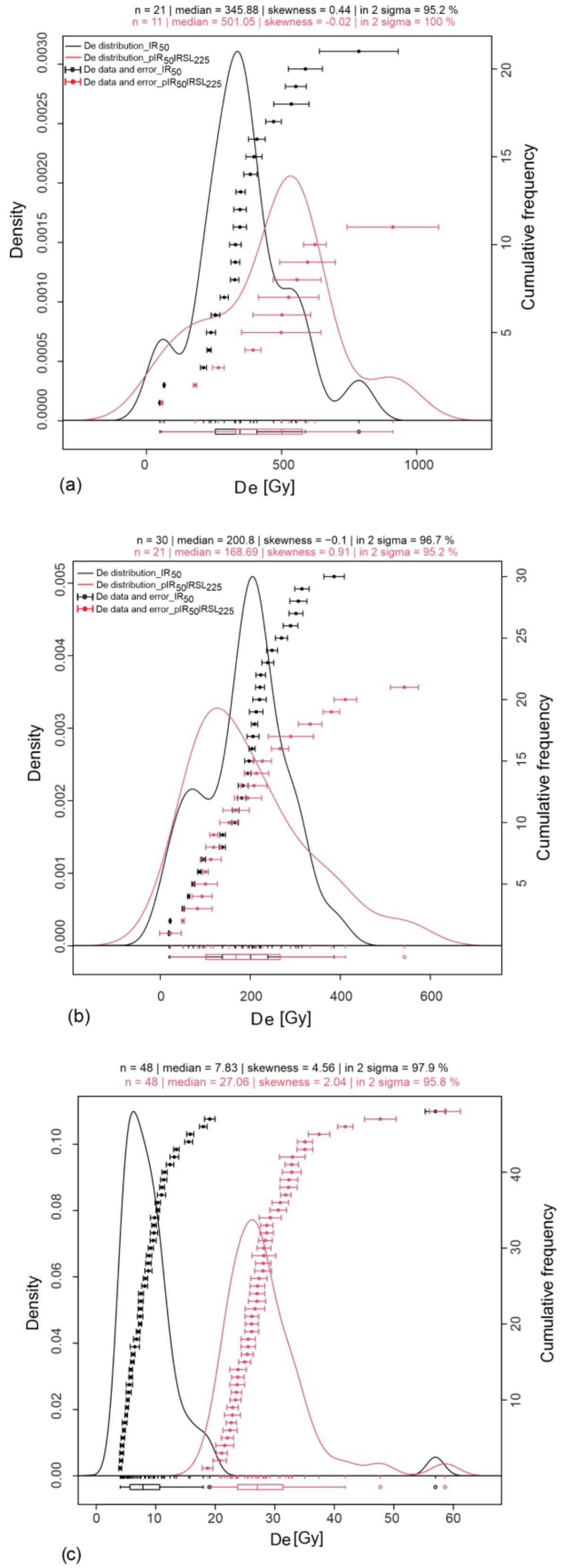

Fig. 6. *Kernal density estimate (Dietze, 2023) plots of equivalent dose (D_e) distributions of the IR_{50} (black dots) and pIR_{50} $IRSL_{225}$ (red dots) signals for samples L2 (a), L3 (b) and L6 (c).*

Table 2. *Summary of age calculation using the MAM and ADM and comparison between IR_{50} and $pIR_{50}IRSL_{225}$ signals. MAM ages of all samples except the $pIR_{50}IRSL_{225}$ age of sample L6 are shown in* ***Fig. 8****.*

IR_{50}

Sample Code	D_e (Gy) MAM	D_e (Gy) ADM	$^*n_a/n_m$	OD (%)	$^{**}\sigma_b$	g_{2days} (%/dec)	n/N	$(n/N)_{ss}$	Age (ka) MAM	Age (ka) ADM	Age fading-corrected (ka) MAM	Age fading-corrected (ka) ADM
L7	4.84 ± 0.86	13.96 ± 1.81	43/48	71 ± 8	0.3	7.87 ± 3.22	0.01 ± 0.00	0.2 ± 0.02	3 ± 1	8 ± 1	8 ± 4	26 ± 17
L6	6.64 ± 0.95	8.85 ± 0.83	48/48	49 ± 5	0.3	6.67 ± 1.29	0.00 ± 0.00	0.04 ± 0.01	4 ± 1	5 ± 1	8 ± 3	11 ± 5
L5	12.80 ± 2.24	52.04 ± 6.30	45/48	81 ± 9	0.3	7.29 ± 1.49	0.01 ± 0.00	0.21 ± 0.02	7 ± 1	28 ± 4	18 ± 10	83 ± 61
L4	13.99 ± 3.83	185.50 ± 18.52	38/48	92 ± 11	0.3	0.87 ± 0.71	0.03 ± 0.01	0.82 ± 0.52	10 ± 3	131 ± 13	10 ± 3	142 ± 18
L3	40.40 ± 9.86	192.83 ± 17.35	30/48	72 ± 6	0.3	3.19 ± 0.94	0.09 ± 0.08	0.52 ± 0.12	29 ± 7	137 ± 13	40 ± 12	198 ± 34
L2	345.03 ± 48.49	361.41 ± 28.23	19/32	31 ± 5	0.3	2.87 ± 1.51	0.54 ± 0.03	0.57 ± 0.16	158 ± 23	166 ± 14	219 ± 68	230 ± 64
L1	173.24 ± 25.67	240.37 ± 15.72	37/48	39 ± 5	0.3	3.18 ± 0.46	0.35 ± 0.08	0.53 ± 0.16	142 ± 22	197 ± 15	204 ± 35	285 ± 29

$pIR_{50}IRSL_{225}$

Sample Code	D_e (Gy) MAM	D_e (Gy) ADM	$^*n_a/n_m$	OD (%)	$^{**}\sigma_b$	g_{2days} (%/dec)	n/N	$(n/N)_{ss}$	Age (ka) MAM	Age (ka) ADM	Age fading-corrected (ka) MAM	Age fading-corrected (ka) ADM
L7	18.01 ± 2.58	33.22 ± 4.79	43/48	67 ± 7	0.3	3.99 ± 1.49	0.06 ± 0.01	0.44 ± 0.15	11 ± 2	19 ± 3	16 ± 5	30 ± 10
L6	27.01 ± 1.34	27.82 ± 0.87	48/48	21 ± 1	-	2.31 ± 1.20	0.05 ± 0.00	0.62 ± 0.24	-	16 ± 2	-	19 ± 4
L5	33.75 ± 4.71	56.10 ± 6.45	37/48	56 ± 7	0.3	1.88 ± 0.36	0.06 ± 0.01	0.59 ± 0.21	18 ± 3	30 ± 3	23 ± 4	40 ± 5
L4	38.21 ± 8.60	218.17 ± 23.88	25/48	80 ± 11	0.3	1.16 ± 0.37	0.09 ± 0.01	0.62 ± 0.45	27 ± 6	154 ± 17	30 ± 7	172 ± 20
L3	86.70 ± 20.70	198.58 ± 27.15	21/48	60 ± 10	0.3	2.59 ± 1.71	0.39 ± 0.05	0.73 ± 0.40	62 ± 15	141 ± 21	90 ± 27	162 ± 40
L2	307.74 ± 87.82	478.05 ± 65.72	10/32	43 ± 11	0.3	0.60 ± 0.89	0.62 ± 0.09	0.82 ± 0.55	142 ± 40	220 ± 30	150 ± 46	233 ± 40
L1	208.35 ± 51.98	297.41 ± 36.87	12/48	40 ± 10	0.3	0.35 ± 0.70	0.65 ± 0.11	0.72 ± 0.54	171 ± 43	244 ± 33	177 ± 47	252 ± 40

* *n_a/n_m = Number of accepted aliquots (n_a) / number of measured aliquots (n_m)*
** *σ_b = Sigma-b*

with those calculated for athermal steady-state $(n/N)_{ss}$ shows that for sample L1 the IR_{50} and $pIR_{50}IRSL_{225}$ and for sample L2 the IR_{50} signal are close to and already in field saturation (>86% of the calculated $(n/N)_{ss}$) (see **Table 2** and **Fig. S7**).

4.3. Dose rate and age results

Results of the dose rate calculation are given in **Table 1**. Analysis of the ^{238}U decay chain (i.e. activity of isotopes ^{226}Ra, ^{214}Pb and ^{214}Bi) indicates secular equilibrium. Investigation of the sensitivity of the environmental dose rate to the water content indicates an age change of 7–10% for a change in water content of 5–20%, hence the ages do not vary beyond their uncertainties.

We explored the environmental dose rate variability with different internal K-contents (12.5%, 8%, 5% and 2%) using DRAC (v1.2; Durcan *et al.*, 2015). The results show that ages increase by ~3% for every 1% reduction in the internal K-content, see **Table S3**.

Fading-corrected IR_{50} ages range between 9 ± 3 ka and 237 ± 25 ka (ADM) compared to 7 ± 3 and 197 ± 61 ka (MAM), and for the $pIR_{50}IRSL_{225}$ signal from 27 ± 9 to 210 ± 36 ka (ADM) compared to 14 ± 5 and 147 ± 39 ka (MAM) (**Table 2**). The ADM ages are systematically older compared to MAM ages (**Fig. 7** and **Fig. S8**). Fading-corrected IR_{50} MAM ages are stratigraphically inconsistent (although neighbouring ages overlap within uncertainty), whereas the ADM ages are more consistent. In contrast, fading-corrected $pIR_{50}IRSL_{225}$ ages are generally stratigraphically consistent for both the MAM and ADM (**Fig. 8** and **Table 2**).

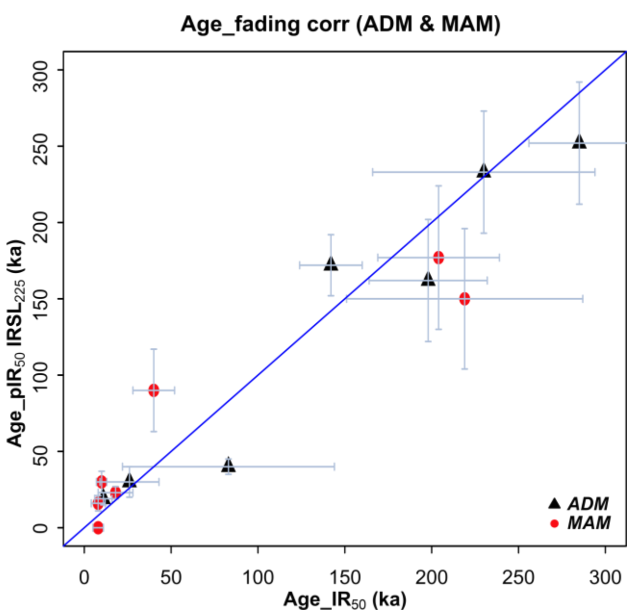

Fig. 7. *Comparison of fading-corrected IR_{50} and $pIR_{50}IRSL_{225}$ ages calculated with the ADM and the MAM.*

5. Discussion

5.1. Luminescence dating of fluvial deposits in Indonesia

Application of luminescence dating in Indonesia has been shown to be challenging (Westaway, 2009) and our quartz luminescence measurements yielded complex properties. We stimulated our quartz samples with blue

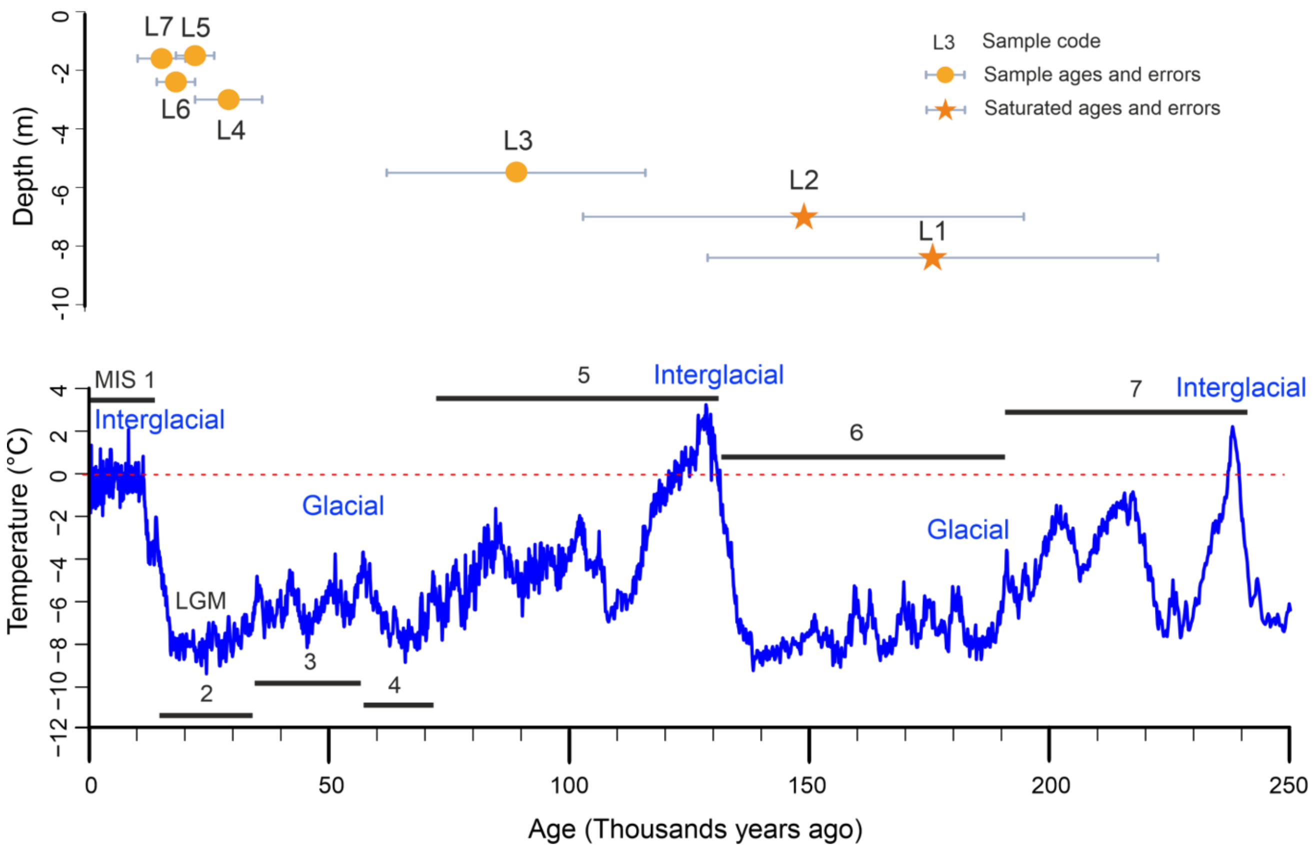

Fig. 8. *Luminescence chronology relative to changing climate and Marine Isotope Stages (MIS). Temperature record and MIS of the last 250 ka modified from Railsback et al. (2015).*

(~400 nm) and green LEDs (~500 nm), but were unable to isolate a fast component (**Fig. 3**). The blue and green stimulated OSL signals are not suitable for dating, as the signals are dim and dominated by slower signal components (i.e., medium and slow components), which may be thermally unstable and could lead to age underestimation (e.g., Steffen *et al.*, 2009). Furthermore, the IR response of the quartz minerals may complicate their dating although we did not explore this further given that the samples were not fast component dominated. Thus, quartz cannot be used for dating sediments from the Kampar Kanan River.

The feldspars under investigation showed suitable luminescence properties with signals brighter than for OSL of quartz, although the amount of sensitive feldspar grains was limited. Although we analysed multiple grains, because of the limited amount of feldspar in our samples, the total signal is presumably dominated by that of 1–5 grains on a multi-grain aliquot, dependent on sample and grain size. Low residual doses (<1% of the natural signal) and successful dose recovery indicate the suitability of the pIR-IRSL protocol for MG K-feldspar used in this study. This is in agreement with previous studies in West Sumatra (Westaway *et al.*, 2017; Duval *et al.*, 2021).

Interpreting the distribution of D_e values for the different samples is challenging, except for sample L6, which shows a log-normal distribution (**Fig. 6** and **Fig. S3**). Most of the dose distributions for the samples investigated have a pattern of positive skewness (**Fig. 6**) and high OD values. These are typical of heterogeneously bleached sediments (Bejarano-Arias *et al.*, 2023) and suggest that the MAM is appropriate. For samples L1 and L2, the field saturation test indicates that these samples are either saturated, or close to saturation (**Table 2** and **Fig. S3**). Thus, the MAM gives minimum ages for those samples. In contrast to the other samples investigated, the post-IR IRSL signal of sample L6 has an OD of only 21 ± 1 % and, thus, the ADM age is used for this signal of this sample. Furthermore, ADM ages are likely to overestimate the depositional age for most of the samples, because of the high likelihood of heterogeneous bleaching in fluvial environments (Olley *et al.*, 1998; Stokes *et al.*, 2001; Wallinga, 2002; Jain *et al.*, 2004; Duller, 2008; Rittenour, 2008). Consequently, the MAM was used for samples L3, L4, L5 and L7, which gave high OD values (≥ 50%). These ages may still overestimate the true burial age of the specific samples because the sediments were likely incompletely bleached. Whilst reduced bleaching of pIR$_{50}$IRSL$_{225}$ signals potentially causes age overestimation, the high fading rates of many of the IR$_{50}$ signals likely make them less reliable. Consequently, we opt to use the fading-corrected pIR$_{50}$IRSL$_{225}$

ages. Despite the challenging sample properties, these ages provide a first chronological framework for the Kampar Kanan River.

5.2. First indications for the Pleistocene evolution of the upper Kampar Kanan River reach

Luminescence dating of the Kampar Kanan River terrace profile provides a chronology of fluvial sediment deposition during the Middle to Late Pleistocene and gives first insights into phases of fluvial adjustments. Given the saturated luminescence signals, the lowermost samples L1 and L2 yield only minimum ages of ~177 ka and ~150 ka, respectively, indicating fluvial aggradation during MIS 6 or earlier (**Fig. 8**). The overlying sediment layer is dated to 90 ± 27 ka in its lower part (sample L3) revealing fluvial deposition during the outgoing phase of the last interglacial and/or MIS 5 (given the large associated uncertainty of the luminescence age). Pollen assemblages and oxygen isotopic measurements in southwest Sumatra (Van Der Kaars *et al.*, 2010) reported generally drier conditions and weaker monsoon intensity during MIS 5a and indicated both vegetation and climate remained similar during MIS 4 and earliest part of MIS 3. Unit 3 is characterized by a fining upward sequence indicative of reducing fluvial energy and decreasing aggradation (Wang *et al.*, 2021), which might represent more stable conditions at this location of the Kampar Kanan River floodplain (e.g. Vandenberghe, 1995; Bogaart *et al.*, 2003; Wang *et al.*, 2015, Wang *et al.*, 2021).

The overlying sample L4 is dated to *ca.* 30 ka showing a gap of approx. 60 ka between units 3 and 4. During MIS 3/2, the cooling climate was likely associated with lower rates of sediment deposition (e.g., van der Kaars, 2010). During this period the summer monsoon became stronger, increasing stream discharge and delaying vegetation recovery (Wang *et al.*, 2021). Unit 3 shows finer sediments indicative of overbank fines in the terrace sequence. Samples L5 to L7 were deposited during MIS2, the last glacial maximum (LGM), characterized by reduced temperatures and increased humidity (van der Kaarst *et al.*, 2010) The upper units are characterized by medium to coarse sand with fine-grained sediments likely accumulating during overbank flooding at times of high monsoon precipitation such that fine sediment deposition on the floodplain at a low rate occurred coincident with slight incision (e.g. Vandenberghe, 1995; Wang *et al.*, 2019; Wang *et al.*, 2021).

From these samples, we interpret that aggradation during climate transitions from cold to warm periods resulted in mixed sand-gravel beds indicating braided river channel development and traction-current gravel facies under predominately cold climatic conditions (e.g. Wang *et al.*, 2015; Gao *et al.*, 2016; Wang *et al.*, 2021). Frequent channel migration under high-energy flow conditions may be due to decreasing vegetation cover and more intense slope erosion resulting in increasing sediment supply (e.g. Bridgland and Westaway, 2008; Lewin and Gibbard, 2010; Stokes *et al.*, 2017., Wang *et al.*, 2021). The abandonment of the overbank fines is characterized by soil formation on top of the sediment sequence, showing more stable conditions in this particular area and highlighting increased incision of the river.

6. Conclusion

Analysis of a suite of samples from a fill terrace of the Kampar Kanan River showed that the OSL of quartz measured using blue or green stimulation as well as SAR or double SAR protocols is not suitable due to IR sensitivity and the absence of a fast component. In contrast, $pIR_{50}IRSL_{225}$ dating of MG K-feldspar yielded a stratigraphically consistent chronology between MIS 6 or earlier to MIS 1, although anomalous fading and partial bleaching of fluvial sediments remain challenging for dating. Luminescence dating and sedimentological analyses show that the Kampar Kanan River aggrades during climate transitions from wet to dry periods, suggesting a significant increase in sediment supply and/or reduced transport capacity.

Acknowledgements

This research was partially supported by Universitas Islam Riau (UIR). We thank the Laboratory of Geological Engineering – UIR (Adi Suryadi and Bayu Harpani) which helped us with the sedimentological analysis. Also, we thank the field assistants who helped us in the field with administration and permit with Kampar Regency (Abdurrahman and Adriyadhi) and collecting luminescence and sedimentological samples (thanks to Tristan, Revanda, Peter, Ziadul Faiez and Gilang) and also shipping the sample from Indonesia to Switzerland.

Supplementary material

Supplementary material containing additional information as well as additional **Figures S1–S8** and **Tables S1–S5** is available online at https://doi.org/10.20858/geochr/205688.

References

Auclair M, Lamothe M and Huot S, 2003. Measurement of anomalous fading for feldspar IRSL using SAR. *Radiation Measurements* 37(4–5): 487–492, DOI 10.1016/S1350-4487(03)00018-0.

Autzen M, Andersen CE, Bailey M and Murray AS, 2022. Calibration quartz: An update on dose calculations for luminescence dating. *Radiation Measurements* 157: 106828, DOI 10.1016/j.radmeas.2022.106828.

Bailey M, Shipley DR and Manning JW, 2015. Roos and NACP-02 ion chamber perturbations and water-air stopping-power ratios for clinical electron beams for energies from 4 to 22 MeV. *Phys. Med. Biol.* 60(3): 1087–1105, DOI 10.1088/0031-9155/60/3/1087.

Balescu S and Lamothe M, 1994. Comparison of TL and IRSL age estimates of feldspar course grains from waterlain sediments. *Quaternary Science Reviews* 13(5–7): 437–444, DOI 10.1016/0277-3791(94)90056-6.

Banerjee D, Murray AS, Bøtter-Jensen L and Lang A, 2001. Equivalent dose estimation using a single aliquot of polymineral fine grains. *Radiation Measurements* 33(1): 73–94, DOI 10.1016/S1350-4487(00)00101-3.

Bejarano-Arias I, Van Wees RMJ, Alexanderson H, Janočko J and Perić Z.M, 2023. Testing the Applicability of Quartz and Feldspar for Luminescence Dating of Pleistocene Alluvial Sediments in the Tatra Mountain Foothills, Slovakia. *Geochronometria* 5(1): 50–80, DOI 10.2478/geochr-2023-0002.

Blong RJ and Gillespie R, 1978. Fluvially transported charcoal gives erroneous 14C ages for recent deposits. *Nature* 271: 739–741, DOI 10.1038/271739a0.

Bogaart PW, Tucker GE and De Vries JJ, 2003. Channel network morphology and sediment dynamics under alternating periglacial and temperate regimes: a numerical simulation study. *Geomorphology* 54(3–4): 257–277, DOI 10.1016/S0169-555X(02)00360-4.

Bridgland D and Westaway R, 2008. Climatically controlled river terrace staircases: A worldwide Quaternary phenomenon. *Geomorphology* 98(3–4): 285–315, DOI 10.1016/j.geomorph.2006.12.032.

Burow C, 2023. calc_MinDose(): Apply the (un-)logged minimum age model (MAM) after Galbraith et al. (1999) to a given De distribution. Function version 0.4.4. In: Kreutzer, S, Burow, C, Dietze, M, Fuchs, M.C, Schmidt, C, Fischer, M, Friedrich, J, Mercier, N, Philippe, A, Riedesel, S, Autzen, M, Mittelstrass, D, Gray, H.J, Galharret, J, 2023. Luminescence: Comprehensive Luminescence Dating Data Analysis. R package version 0.9.22.

Burow C, 2025. calc_AliquotSize(): Estimate the amount of grains on an aliquot. Function version 0.31. In: Kreutzer, S, Burow, C, Dietze, M, Fuchs, M.C, Schmidt, C, Fischer, M, Friedrich, J, Mercier, N, Philippe, A, Riedesel, S, Autzen, M, Mittelstrass, D, Gray, H.J, Galharret, J, Colombo, M, Steinbuch, L, Boer, A.d, 2025. Luminescence: Comprehensive Luminescence Dating Data Analysis. R package version 1.0.1.

Buylaert JP, Murray AS, Thomsen KJ and Jain M, 2009. Testing the potential of an elevated temperature IRSL signal from K-feldspar. *Radiation Measurements* 44(5–6): 560–565, DOI 10.1016/j.radmeas.2009.02.007.

Choanji T, 2019. Clustering Slope Stability Using Dem Lineament Extraction And Rock Mass Rating In Pangkalan Koto Baru, West Sumatra, Indonesia. *GEOMATE* 17(60): 225–230, DOI 10.21660/2019.60.ICEE21.

Choanji T, 2017. Slope Analysis Based On SRTM Digital Elevation Model Data: Study Case On Rokan IV Koto Area And Surrounding. *Journal of Dynamics* 1: 71–75.

Choi J, Chamberlain E and Wallinga J, 2024. Variance in pIRIR signal bleaching for single grains of feldspar. *Quaternary Geochronology* 83: 101577, DOI 10.1016/j.quageo.2024.101577.

Christophe C, Philippe A and Kreutzer S, 2023. calc_AverageDose(): Calculate the Average Dose and the Dose Rate Dispersion. Function Version 0.1.5. In: Kreutzer S, Burow C, Dietze M, Fuchs M C, Schmidt C, Fischer M, Friedrich J, Mercier N, Philippe A, Riedesel S, Autzen M, Mittelstrass D, Gray H J, Galharret J, 2023. Luminescence : Comprehensive Luminescence Dating Data Analysis. R Package Version 0.9.22. https://CRAN.R-project.org/package=Luminescence.

Clarke MCG, Kartawa W, A Djunuddin E, Suganda E and Bagdja M, 1982. Geological Map of The Pakanbaru Quadrangle, Sumatera, Scale 1 : 250.000. Geological Research and Development Centre, Bandung.

Cunha PP, Martins AA, Huot S, Murray A and Raposo L, 2008. Dating the Tejo river lower terraces in the Ródão area (Portugal) to assess the role of tectonics and uplift. *Geomorphology* 102(1): 43–54, DOI 10.1016/j.geomorph.2007.05.019.

Cunningham AC and Wallinga J, 2012. Realizing the potential of fluvial archives using robust OSL chronologies. Quaternary *Geochronology* 12: 98–106, DOI 10.1016/j.quageo.2012.05.007.

Dietze M, 2023. plot_KDE(): Plot kernel density estimate with statistics. Function version 3.6.0. In: Kreutzer S, Burow C, Dietze M, Fuchs MC, Schmidt C, Fischer M, Friedrich J, Mercier N, Philippe A, Riedesel S, Autzen M, Mittelstrass D, Gray HJ, Galharret J, 2023. *Luminescence: Comprehensive Luminescence Dating Data Analysis* . R package version 0.9.22, DOI 10.5281/zenodo.7467059.

Duller GAT, 2008. Single-grain optical dating of Quaternary sediments: why aliquot size matters in luminescence dating. *Boreas* 37(4): 589–612, DOI 10.1111/j.1502-3885.2008.00051.x.

Duller GAT, 2003. Distinguishing quartz and feldspar in single grain luminescence measurements. *Radiation Measurements* 37(2): 161–165, DOI 10.1016/S1350-4487(02)00170-1.

Duller GAT, 1992. Luminescence Chronology of Raised Marine Terraces, South-West North Island, New Zealand. PhD thesis, Institute of Earth Studies, University of Wales, Aberystwyth.

Durcan JA, King GE and Duller GAT, 2015. Quaternary Geochronology DRAC : Dose Rate and Age Calculator for trapped charge dating. *Quaternary Geochronology* 28: 54–61, DOI 10.1016/j.quageo.2015.03.012.

Duval M, Westaway K, Zaim J, Rizal Y, Aswan, Puspaningrum MR, Trihascaryo A, Albers PCH, Smith HE, Drawhorn GM, Price GJ and Louys J, 2021. New Chronological Constraints for the Late Pleistocene Fossil Assemblage and Associated Breccia from Ngalau Sampit, Sumatra. *Open Quaternary* 7(1): 1–24, DOI 10.5334/oq.96.

Galbraith RF, Roberts RG, Laslett GM, Yoshida H and Olley JM, 1999. Optical dating of single and multiple grains of quartz from Jinmium rock shelter, northern Australia: Part I, experimental design and statistical models. *Archaeometry* 41(2): 339–364, DOI 10.1111/j.1475-4754.1999.tb00987.x.

Gao H, Li Z, Pan B, Liu F and Liu X, 2016. Fluvial responses to late Quaternary climate change in the Shiyang River drainage system, western China. *Geomorphology* 258: 82–94, DOI 10.1016/j.geomorph.2016.01.018.

Guérin G, Christophe C, Philippe A, Murray AS, Thomsen KJ, Tribolo C, Urbanova P, Jain M, Guibert P, Mercier N, Kreutzer S and Lahaye C, 2017. Absorbed dose, equivalent dose, measured dose rates, and implications for OSL age estimates: Introducing the Average Dose Model. *Quaternary Geochronology* 41: 163–173, DOI 10.1016/j.quageo.2017.04.002.

Guérin G, Mercier N and Adamiec G, 2011. Dose-rate conversion factors: update. *Ancient* TL 29(1): 5–8, DOI 10.26034/la.atl.2011.443.

Guérin G, Mercier N, Nathan R, Adamiec G and Lefrais Y, 2012. On the use of the infinite matrix assumption and associated concepts: A critical review. *Radiation Measurements* 47(9): 778–785, DOI 10.1016/j.radmeas.2012.04.004.

Guralnik B, Ankjærgaard C, Jain M, Murray AS, Müller A, Wälle M, Lowick SE, Preusser F, Rhodes EJ, Wu TS, Mathew G and Herman F, 2015. OSL-thermochronometry using bedrock quartz: A note of caution. *Quaternary Geochronology* 25: 37–48, DOI 10.1016/j.quageo.2014.09.001.

Hansen V, Murray A, Buylaert JP, Yeo EY and Thomsen K, 2015. A new irradiated quartz for beta source calibration. *Radiation Measurements* 81: 123–127, DOI 10.1016/j.radmeas.2015.02.017.

Heitmuller FT and Hudson PF, 2009. Downstream trends in sediment size and composition of channel-bed, bar, and bank deposits related to hydrologic and lithologic controls in the Llano River watershed, central Texas, USA. *Geomorphology* 112(3–4): 246–260, DOI 10.1016/j.geomorph.2009.06.010.

Heidrick TL and Aulia K, 1993. A Structural and Tectonic Model of The Coastal Plain Block, Central Sumatra Basin, Indonesia. *Proceeding IPA* 22th *Annual Convention, Jakarta*.

Huntley DJ, 2006. An explanation of the power-law decay of luminescence. *Journal of Physics: Condensed Matter* 18: 1359–1365, DOI 10.1088/0953-8984/18/4/020.

Huntley DJ and Baril MR, 1997. The K content of the K-feldspars being measured in optical dating or in thermoluminescence dating. *Ancient TL* 15(1): 11–13, DOI 10.26034/la.atl.1997.271.

Huntley DJ and Lamothe M, 2001. Ubiquity of anomalous fading in K-feldspars and the measurement and correction for it in optical dating. *Canadian Journal of Earth Sciences* 38(7): 1093–1106, DOI 10.1139/e01-013.

Jain M, Murray AS and Btter-Jensen L, 2004. Optically stimulated luminescence dating: How significant is incomplete light exposure in fluvial environments?. *Quaternaire* 15(1–2): 143–157.

Kaharudin HAF, Alifah A, Ramadhan L and Kealy S, 2020. A review of archaeological dating efforts at cave and rockshelter sites in the Indonesian Archipelago. *JIPA* 44: 80–112, DOI 10.7152/jipa.v44i0.15659.

Kars RH, Wallinga J and Cohen KM, 2008. A new approach towards anomalous fading correction for feldspar IRSL dating — tests on samples in field saturation. *Radiation Measurements* 43(2–6): 786–790, DOI 10.1016/j.radmeas.2008.01.021.

Kausarian H, Josaphat Tetuko Sri Sumantyo, Batara, Suryadi A and Pangestu T, 2024. SAR Sentinel Data Analysis: Hydrological Dynamics and Rainfall Patterns in the Kampar River Basin (2018-2023). *Evergreen* 11(3): 1558–1567, DOI 10.5109/7236811.

King GE and Burow C, 2023. calc_Huntley2006(): Apply the Huntley (2006) model. Function version 0.4.1. In: Kreutzer, S, Burow, C, Dietze, M, Fuchs, M.C, Schmidt, C, Fischer, M, Friedrich, J, Mercier, N, Philippe, A, Riedesel, S, Autzen, M, Mittelstrass, D, Gray, H.J, Galharret, J, 2023. Luminescence: Comprehensive Luminescence Dating Data Analysis. R package version 0.9.22.

King GE, Burow C, Roberts HM and Pearce NJG, 2018. Age determination using feldspar: Evaluating fading-correction model performance. *Radiation Measurements* 119: 58–73, DOI 10.1016/j.radmeas.2018.07.013.

Knox JC, 2006. Floodplain sedimentation in the Upper Mississippi Valley: Natural versus human accelerated. *Geomorphology* 79(3–4): 286–310, DOI 10.1016/j.geomorph.2006.06.031.

Koesoemadinata RP and Matasak T, 1981. Stratigraphy and sedimentation Ombilin Basin, Central Sumatra (West Sumatra Province). *Proc. Indones. Pet. Assoc. Tenth Annu. Conv*: 217–250.

Kreutzer S and Burow C, 2023. analyse_FadingMeasurement(): Analyse fading measurements and returns the fading rate per decade (g-value). Function version 0.1.21. In: Kreutzer, S, Burow, C, Dietze, M, Fuchs, M.C, Schmidt, C, Fischer, M, Friedrich, J, Mercier, N, Philippe, A, Riedesel, S, Autzen, M, Mittelstrass, D, Gray, H.J, Galharret, J, 2023. https://CRAN.R-project.org/package=Luminescence.

Kreutzer S, Burow C, Dietze M, Fuchs M C, Schmidt C, Fischer M, Friedrich J, Mercier N, Philippe A, Riedesel S, Autzen M, Mittelstrass D, Gray H J, Galharret J-M, 2023. Luminescence: Comprehensive Luminescence Dating Data Analysis . R Package Version 0.9.22. https://CRAN.R-project.org/package=Luminescence.

Kreutzer S, Schmidt C, Fuchs MC, Dietze M, Fischer M and Fuchs M, 2012. Introducing an R package for luminescence dating analysis. *Ancient TL* 30(1): 1–8, DOI 10.26034/la.atl.2012.457.

Krüger J and Kjær KH, 1999. A data chart for field description and genetic interpretation of glacial diamicts and associated sediment with examples from Greenland, Iceland, and Denmark. *Boreas* 28(3): 386–402, DOI 10.1111/j.1502-3885.1999.tb00228.x.

Lewin J and Gibbard PL, 2010. Quaternary river terraces in England: Forms, sediments and processes. *Geomorphology* 120(3–4): 293–311, DOI 10.1016/j.geomorph.2010.04.002.

Linsley BK, Rosenthal Y and Oppo DW, 2010. Holocene evolution of the Indonesian throughflow and the western Pacific warm pool. *Nature Geoscience* 3: 578–583, DOI 10.1038/ngeo920.

Louys J, Kealy S, O'Connor S, Price G, Hawkins S, Aplin K, Rizal Y, Zaim J, Mahirta, Tanudirjo D, Santoso WD, Hidayah AR, Trihascaryo A, Wood R, Bevitt J and Clark T, 2017. Differential preservation of vertebrates in Southeast Asian caves. *International Journal of Speleology* 46: 379–408, DOI 10.5038/1827-806X.46.3.2131.

Macklin MG, Lewin J and Woodward JC, 2012. The fluvial record of climate change. *Philosophical Transactions of the Royal Society A: Mathematical, Physical and Engineering Sciences* 370: 2143–2172, DOI 10.1098/rsta.2011.0608.

Miall AD, 1985. Architectural-element analysis: a new method of facies analysis applied to fluvial deposits. *Earth-Science Reviews* 22(4): 261–308, DOI 10.1016/0012-8252(85)90001-7.

Mishra K and Sinha R, 2020. Flood risk assessment in the Kosi megafan using multi-criteria decision analysis: A hydro-geomorphic approach. *Geomorphology* 350: 106861, DOI 10.1016/j.geomorph.2019.106861.

Morley R, 2017. Constructing Neogene palaeogeographical maps for the Sunda region. SEAPEX Exploration Conference, Singapore, 1–7.

Murray AS and Wintle AG, 2000. Luminescence dating of quartz using an improved single-aliquot regenerative-dose protocol. *Radiation Measurements* 32(1): 57–73, DOI 10.1016/S1350-4487(99)00253-X.

Olley J, Caitcheon G and Murray A, 1998. The distribution of apparent dose as determined by optically stimulated luminescence in small aliquots of fluvial quartz: Implications for dating young sediments. *Quaternary Science Reviews* 17(11): 1033–1040, DOI 10.1016/S0277-3791(97)00090-5.

O'Gorman K, Tanner D, Sontag-González M, Li B, Brink F, Jones BG, Dosseto A, Jatmiko, Roberts RG and Jacobs Z, 2021. Composite grains from volcanic terranes: Internal dose rates of supposed 'potassium-rich' feldspar grains used for optical dating at Liang Bua, Indonesia. *Quaternary Geochronology* 64: 101182, DOI 10.1016/j.quageo.2021.101182.

Prescott JR and Hutton JT, 1994. Cosmic ray contributions to dose rates for luminescence and ESR dating: Large depths and long-term time variations. *Radiation Measurements* 23(2–3): 497–500, DOI 10.1016/1350-4487(94)90086-8.

Putra DBE and Choanji T, 2016. Preliminary Analysis of Slope Stability in Kuok and Surrounding Areas. *Journal of Geoscience, Engineering, Environment, and Technology* 1(1): 41–44, DOI 10.24273/jgeet.2016.11.5.

Railsback LB, Gibbard PL, Head MJ, Voarintsoa NRG and Toucanne S, 2015. An optimized scheme of lettered marine isotope substages for the last 1.0 million years, and the climatostratigraphic nature of isotope stages and substages. *Quaternary Science Reviews* 111: 94–106, DOI 10.1016/j.quascirev.2015.01.012.

Revanda M, Yuskar Y, Eka Putra DB and Sari DP, 2019. Quartenary Sediment Facies Distribution in Meandering River Environment: Study Case at the Kampar River, Rumbio Area and Surroundings, Riau Province. *Journal of Physics: Conference Series* 1: 1–7, DOI 10.1088/1742-6596/1363/1/012038.

Riebe CS, Kirchner JW, Granger DE and Finkel RC, 2000. Erosional equilibrium and disequilibrium in the Sierra Nevada, inferred from cosmogenic 26 Al and 10 Be in alluvial sediment. *Geology* 28(9): 803–806, DOI 10.1130/0091-7613(2000)28<803:EEADIT>2.0.CO;2.

Rittenour TM, 2008. Luminescence dating of fluvial deposits: Applications to geomorphic, palaeoseismic and archaeological research. *Boreas* 37(4): 613–635, DOI 10.1111/j.1502-3885.2008.00056.x.

Rixhon G, Briant RM, Cordier S, Duval M, Jones A and Scholz D, 2017. Revealing the pace of river landscape evolution during the Quaternary: recent developments in numerical dating methods. *Quaternary Science Reviews* 166: 91–113, DOI 10.1016/j.quascirev.2016.08.016.

Roberts HM and Wintle AG, 2001. Equivalent dose determinations for polymineralic fine-grains using the SAR protocol: Application to a Holocene sequence of the Chinese Loess Plateau. *Quaternary Science Reviews* 20(5–9): 859–863, DOI 10.1016/S0277-3791(00)00051-2.

Sinha R and Latrubesse EM, 2020. Geomorphology of fluvial systems: Focus on tropical rivers. *Geomorphology* 363: 107223, DOI 10.1016/j.geomorph.2020.107223.

Sinha R, Latrubesse EM and Nanson GC, 2012. Quaternary fluvial systems of tropics: Major issues and status of research. *Palaeogeography, Palaeoclimatology, Palaeoecology* 356–357: 1–15, DOI 10.1016/j.palaeo.2012.07.024.

Smedley RK, Buylaert J-P and Újvári G, 2019. Comparing the accuracy and precision of luminescence ages for partially-bleached sediments using single grains of K-feldspar and quartz. *Quaternary Geochronology* 53: 101007, DOI 10.1016/j.quageo.2019.101007.

Sontag-González M, Li B, O'Gorman K, Sutikna T, Jatmiko, Jacobs Z, Roberts RG, 2021. Establishing a pIRIR procedure for De determination of composite mineral grains from volcanic terranes: A case study of sediments from Liang Bua, Indonesia. *Quaternary Geochronology* 65: 101181, DOI 10.1016/j.quageo.2021.101181.

Stanistreet IG, Cairncross B and McCarthy TS, 1993. Low sinuosity and meandering bedload rivers of the Okavango Fan: channel confinement by vegetated levées without fine sediment. *Sedimentary Geology* 85(1–4): 135–156, DOI 10.1016/0037-0738(93)90079-K.

Stanley DJ, 2000. Holocene Depositional Patterns, Neotectonics and Sundarban Mangroves in the Western Ganges-Brahmaputra Delta. *Journal of Coastal Research* 16(1): 26–39.

Steffen D, Schlunegger F and Preusser F, 2009. Drainage basin response to climate change in the Pisco valley, Peru. *Geology* 37(6): 491–494, DOI 10.1130/G25475A.1.

Stokes S, Bray HE and Blum MD, 2001. Optical resetting in large drainage basins: Tests of zeroing assumptions using single-aliquot procedures. *Quaternary Science Reviews* 20(5–9): 879–885, DOI 10.1016/S0277-3791(00)00045-7.

Stokes M, Mather AE, Belfoul M, Faik F, Bouzid S, Geach MR, Cunha PP, Boulton SJ and Thiel C, 2017. Controls on dryland mountain landscape development along the NW Saharan desert margin: Insights from Quaternary river terrace sequences (Dadès River, south-central High Atlas, Morocco). *Quaternary Science Reviews* 166: 363–379, DOI 10.1016/j.quascirev.2017.04.017.

Syvitski JPM, Cohen S, Kettner AJ and Brakenridge GR, 2014. How important and different are tropical rivers? - An overview. *Geomorphology* 227: 5–17, DOI 10.1016/j.geomorph.2014.02.029.

Sutikna T, Tocheri MW, Morwood MJ, Saptomo EW, Jatmiko, Awe RD, Wasisto S, Westaway KE, Aubert M, Li B, Zhao J, Storey M, Alloway BV, Morley MW, Meijer HJM, Van Den Bergh GD, Grün R, Dosseto A, Brumm A, Jungers WL and Roberts RG, 2016. Revised stratigraphy and chronology for Homo floresiensis at Liang Bua in Indonesia. *Nature* 532: 366–369, DOI 10.1038/nature17179.

Thomas MF, 2008. Understanding the impacts of Late Quaternary climate change in tropical and sub-tropical regions. *Geomorphology* 101(1–2): 146–158, DOI 10.1016/j.geomorph.2008.05.026.

Thomsen KJ, Murray AS, Jain M and Bøtter-Jensen L, 2008. Laboratory fading rates of various luminescence signals from feldspar-rich sediment extracts. *Radiation Measurements* 43(9–10): 1474–1486, DOI 10.1016/j.radmeas.2008.06.002.

Thorp M and Thomas M, 1992. The timing of alluvial sedimentation and floodplain formation in the lowland humid tropics of Ghana, Sierra Leone and western Kalimantan (Indonesian Borneo). *Geomorphology* 4(6): 409–422, DOI 10.1016/0169-555X(92)90035-M.

Van Den Bergh GD, Li B, Brumm A, Grün R, Yurnaldi D, Moore MW, Kurniawan I, Setiawan R, Aziz F, Roberts RG, Suyono, Storey M, Setiabudi E and Morwood MJ, 2016. Earliest hominin occupation of Sulawesi, Indonesia. *Nature* 529: 208–211, DOI 10.1038/nature16448.

Van Der Kaars S, Bassinot F, De Deckker P and Guichard F, 2010. Changes in monsoon and ocean circulation and the vegetation cover of southwest Sumatra through the last 83,000 years: The record from marine core BAR94-42. *Palaeogeography, Palaeoclimatology, Palaeoecology* 296(1–2): 52–78, DOI 10.1016/j.palaeo.2010.06.015.

Vandenberghe J, 1995. Timescales, climate and river development. *Quaternary Science Reviews* 14(6): 631–638, DOI 10.1016/0277-3791(95)00043-O.

Verstappen H, 1980. Quaternary Climatic Changes and Natural Environment in SE Asia. *Geojournal* 4: 45–54, DOI 10.1007/BF00586754.

Wallinga J, 2002. Optically stimulated luminescence dating in fluvial deposits: A review. *Boreas* 31(4): 303–322, DOI 10.1111/j.1502-3885.2002.tb01076.x.

Wang B, Wang X, Yi S, Zhao L and Lu H, 2021. Responses of fluvial terrace formation to monsoon climate changes in the north-eastern Tibetan Plateau: Evidence from pollen and sedimentary records. *Palaeogeography, Palaeoclimatology, Palaeoecology* 564: 110196, DOI 10.1016/j.palaeo.2020.110196.

Wang X, Ma J, Yi S, Vandenberghe J, Dai Y and Lu H, 2019. Interaction of fluvial and eolian sedimentation processes, and response to climate change since the last glacial in a semiarid environment along the Yellow River. *Quartenary Research* 91(2): 570–583, DOI 10.1017/qua.2018.22.

Wang X, Vandenberghe J, Yi S, Van Balen R and Lu H, 2015. Climate-dependent fluvial architecture and processes on a suborbital timescale in areas of rapid tectonic uplift: An example from the NE Tibetan Plateau. *Global and Planetary Change* 133: 318–329, DOI 10.1016/j.gloplacha.2015.09.009.

Westaway KE, 2009. The red, white and blue of quartz luminescence: A comparison of De values derived for sediments from Australia and Indonesia using thermoluminescence and optically stimulated luminescence emissions. *Radiation Measurements* 44(5–6): 462–466, DOI 10.1016/j.radmeas.2009.06.001.

Westaway KE, Louys J, Awe RD, Morwood MJ, Price GJ, Zhao JX, Aubert M, Joannes-Boyau R, Smith TM, Skinner MM, Compton T, Bailey RM, Van Den Bergh GD, De Vos J, Pike AWG, Stringer C, Saptomo EW, Rizal Y, Zaim J, Santoso WD, Trihascaryo A, Kinsley L and Sulistyanto B, 2017. An early modern human presence in Sumatra 73,000-63,000 years ago. *Nature* 548: 322–325, DOI 10.1038/nature23452.

Westaway KE and Roberts RG, 2006. A dual-aliquot regenerative-dose protocol (DAP) for thermoluminescence (TL) dating of quartz sediments using the light-sensitive and isothermally stimulated red emissions. *Quaternary Science Reviews* 25(19–20): 2513–2528, DOI 10.1016/j.quascirev.2005.06.010.

Wisha UJ, Rahmawan GA and Ilham I, 2018. *Bono Kuala Kampar, Primadona di Timur Sumatera Yang Terancam Hilang (*Kuala Kampar's Bono, a favourite in eastern Sumatra, is in danger of disappearing*)*. AMAFRAD Press: Jakarta, Indonesia: 89pp (In Indonesian).

Wisha UJ, Wijaya YJ and Hisaki Y, 2022. Real-Time Properties of Hydraulic Jump off a Tidal Bore, Its Generation and Transport Mechanisms: A Case Study of the Kampar River Estuary, Indonesia. *Water* 14(16): 2561, DOI 10.3390/w14162561.

Wood SH, Ziegler AD and Bundarnsin T, 2008. Floodplain deposits, channel changes and riverbank stratigraphy of the Mekong River area at the 14th-Century city of Chiang Saen, Northern Thailand. *Geomorphology* 101(3): 510–523, DOI 10.1016/j.geomorph.2007.04.030.

Yuskar Y, 2016. Geo-tourism Potential of Sand Bars and Oxbow lake at Buluh Cina, Kampar Riau, Indonesia. *Journal of Geoscience, Engineering, Environtment, and Technology* 1(1): 59–62, DOI 10.24273/jgeet.2016.11.8.

Yuskar Y, Putra DBE and Revanda M, 2018. Quarternary Sediment Characteristics of Floodplain area: Study Case at Kampar River, Rumbio Area and Surroundings, Riau Province. *Journal of Geoscience, Engineering, Environment, and Technology* 3(1): 63–68, DOI 10.24273/jgeet.2018.3.1.1226.

Yuskar Y, Putra DBE, Suryadi A, Choanji T and Cahyaningsih C, 2017. Structural Geology Analysis In A Disaster-Prone Of Slope Failure, Merangin Village, Kuok District, Kampar Regency, Riau Province. *Journal of Geoscience, Engineering, Environment, and Technology* 2(4): 249–254, DOI 10.24273/jgeet.2017.2.4.691.

Zhang JF and Zhou LP, 2007. Optimization of the "double SAR" procedure for polymineral fine grains. *Radiation Measurements* 42(9): 1475–1482, DOI 10.1016/j.radmeas.2007.06.007.